

Figure S1. *MLH1* deficiency induces DNA breaks and activates the cGAS pathway, Related to Figure 1.

(A) Microscopy images showing accumulation of cytosolic DNA (arrows) in *Mlh1*-deficient and MLH1-rescued (Rescd) HCT116 cells with or without IR treatment (10 Gy). Cells were collected 24 h after IR treatment, and DNA was detected using PicoGreen, a fluorescence dye that selectively binds dsDNA. (B) Percentage of the indicated cells displaying cytosolic DNA with and without IR treatment. (C) Western blots showing that *MLH1*-rescue in HCT116 cells reduced IR-induced γ H2AX levels. (D) Three independent HPLC profiles showing cGAMP levels for each cell type, as indicated. (E) qRT-PCR analysis showing increased production of *Irf7* in *Mlh1*^{-/-} 4T1 cells with or without IR. (F) qRT-PCR analysis showing that increased production of *Irf7* in *Mlh1*^{-/-} 4T1 cells depends on cGAS. (G) Western blots showing that enhanced pSTAT1 in *Mlh1*^{-/-} 4T1 cells depend on STING. (H) and (I) qRT-PCR analysis indicating that increased production of *Isg15* and *Irf7* in *Mlh1*^{-/-} 4T1 cells depends on STING, respectively. Data represent the mean \pm SEM of 3 independent experiments (B) or triplicates (E, F, H and I). P value was calculated using one-way ANOVA. **, $p < 0.01$; ****, $p < 0.0001$.

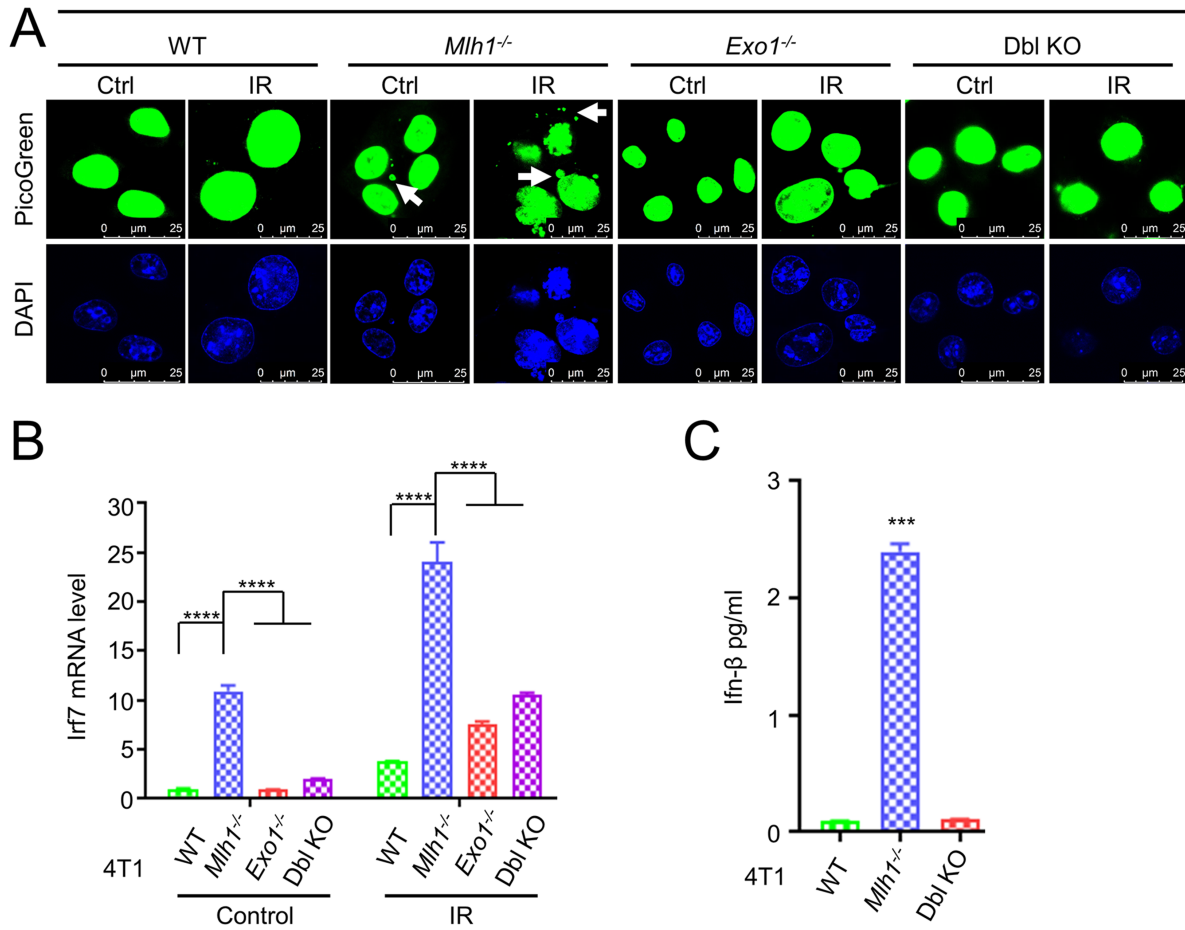


Figure S2. Exo1 is essential for innate sensing signaling in *Mlh1*^{-/-} 4T1 cells, Related to Figure 2.

(A) Depletion of Exo1 reduces cytosolic DNA accumulation in *Mlh1*^{-/-} 4T1 cells regardless of IR treatment. DNA was detected using PicoGreen 24 h post IR. (B) and (C) qRT-PCR analysis demonstrating Exo1 depletion-suppressed upregulation of innate sensing factors Irf7 and Ifn-β, respectively. Data represent the mean ± SEM of triplicates (B and C). P value was calculated using one-way ANOVA. ***, p<0.001; ****, p<0.0001.

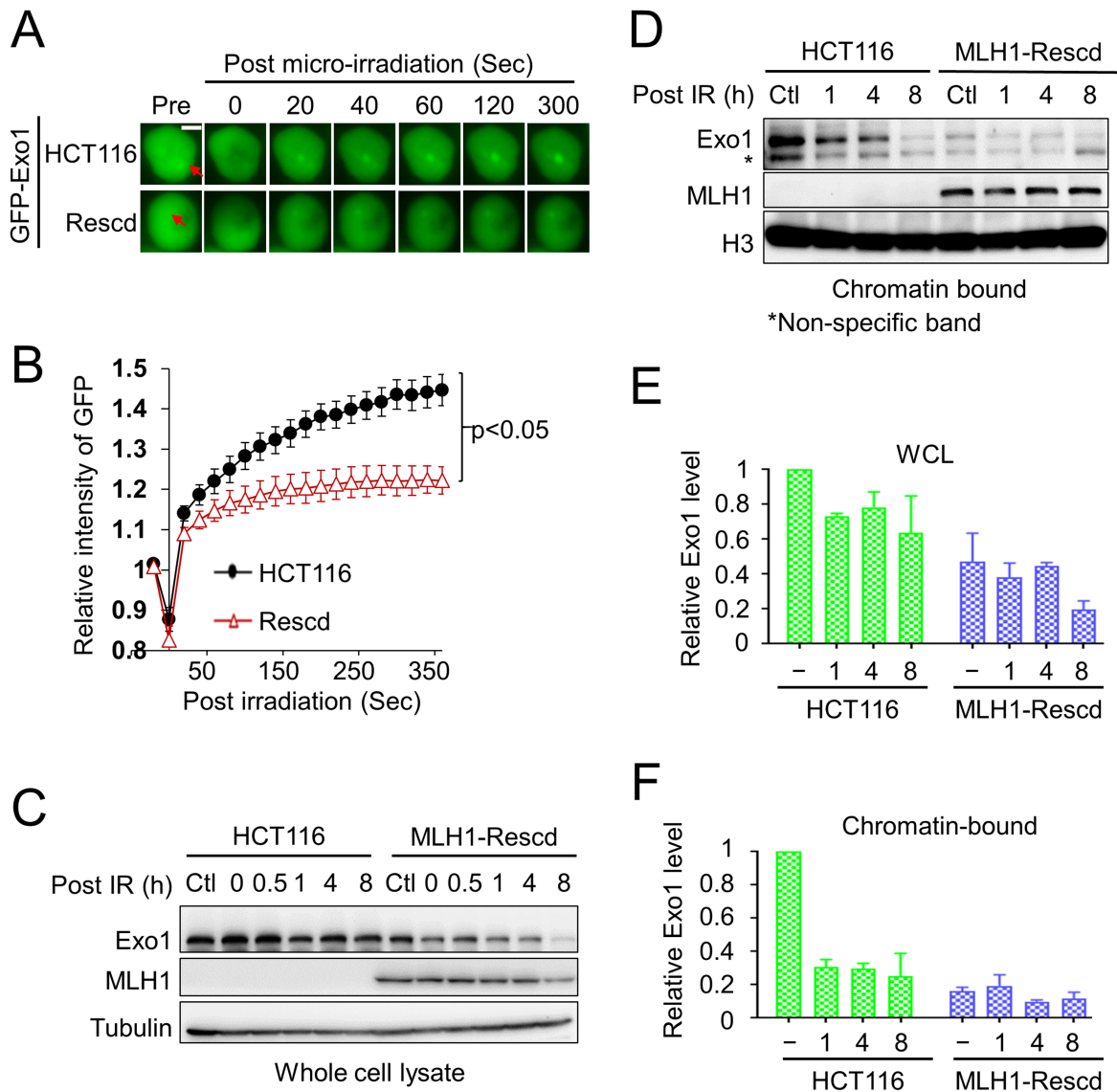


Figure S3. Abundance of Exo1 in *MLH1*^{-/-} cells, Related to Figure 4.

(A) Live cell imaging showing real-time recruitment of GFP-tagged Exo1 in *MLH1*-deficient HCT116 and *MLH1*-rescued HCT116 cells in response to micro-irradiation. (B) Quantification of Exo1 levels at the site of laser micro-irradiation in HCT116 and its *MLH1*-rescued derivative. Relative fluorescent intensity of GFP-Exo1 was presented as mean \pm SEM from 14 HCT116 and 11 *MLH1*-rescued HCT116 cells. (C) and (D) Western blots showing whole cell lysate and chromatin-bound Exo1 levels in HCT116 and *MLH1*-rescued HCT116 cells, respectively. (E) and (F) Quantification of relative Exo1 levels in whole cell lysates and on chromatin, respectively. Data represent the mean \pm SEM of three independent determinants.

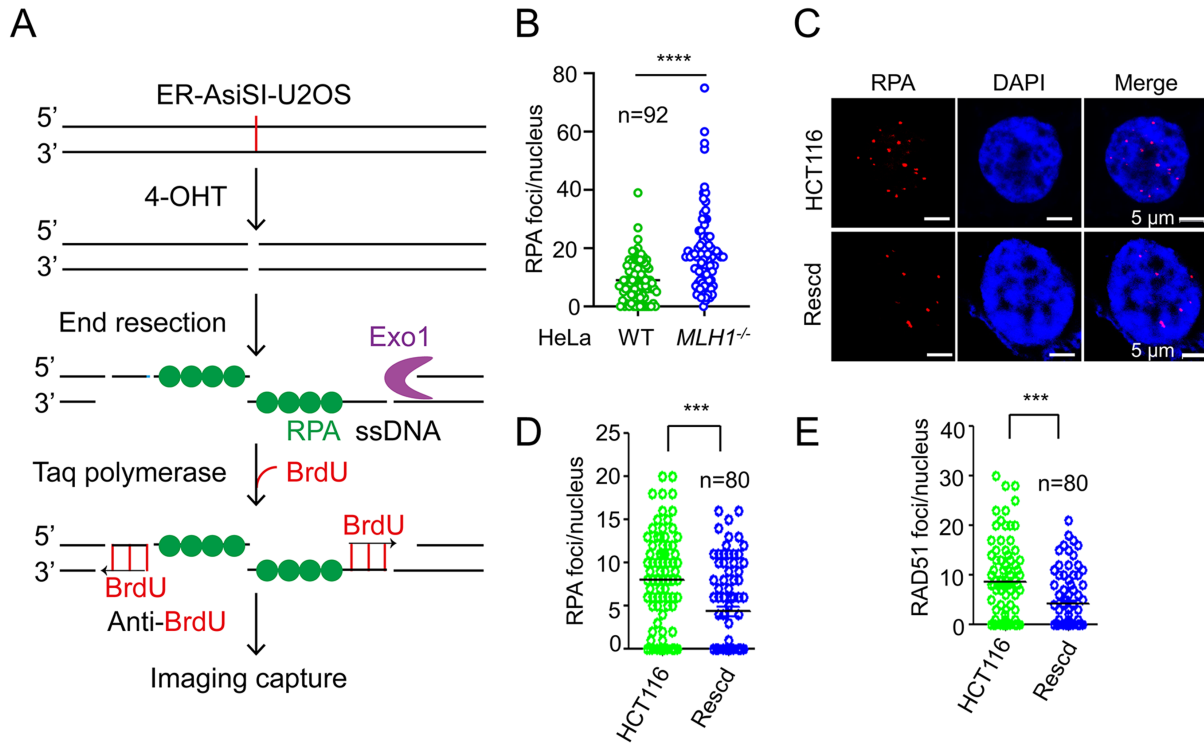


Figure S4. Aberrant end resection-led RPA exhaustion in *MLH1*^{-/-} cells, Related to Figure 5.

(A) Diagram showing the principle of RPA exhaustion assay. 4-OHT treatment specifically leads to DSBs at AsiSI sites. DNA end resection induces ssDNA, which is protected by RPA. When hyper-resection occurs, a large quantity of ssDNAs are generated, which exhausted the RPA pool, resulting in unprotected ssDNA. The unprotected ssDNA can be used as a template for DNA synthesis to incorporate BrdU, which can be visualized by a BrdU-specific antibody. (B) Quantification of RPA foci per nuclei in HeLa and *MLH1*^{-/-} HeLa cells 24 h after IR (10 Gy) treatment. (C) Immunofluorescence confocal analysis showing RPA foci in HCT116 and *MLH1*-rescued HCT116 cells. (D) and (E) Quantification of RPA and RAD51 foci per nuclei, respectively, in HCT116 and *MLH1*-rescued HCT116 cells. Data represent the mean \pm SEM of the indicated number of cells (B, D and E). P value was calculated using one-way ANOVA. ***, $p < 0.001$; ****, $p < 0.0001$.

